Thin Solid Films 529 (2013) 389–393

Contents lists available at SciVerse ScienceDirect

Thin Solid Films

journal homepage: www.elsevier.com/locate/tsf

Investigating bipolar resistive switching characteristics in filament type and interface type BON-based resistive switching memory

Hsueh-Chih Tseng [a], Ting-Chang Chang [a,b,*], Kai-Hung Cheng [c], Jheng-Jie Huang [a], Yu-Ting Chen [c], Fu-Yen Jian [a], Simon M. Sze [a,d,e], Ming-Jinn Tsai [f], Ann-Kuo Chu [c], Ying-Lang Wang [g]

[a] Department of Physics, National Sun Yat-Sen University, Kaohsiung, 804, Taiwan, ROC
[b] Advanced Optoelectronics Technology Center, National Cheng Kung University, 1 Ta-hsueh Road, Tainan 701, Taiwan, ROC
[c] Department of Photonics, National Sun Yat-Sen University, Kaohsiung, 804, Taiwan, ROC
[d] Department of Electrical Engineering, Stanford University, Stanford, CA 94305-4085, USA
[e] Department of Electronics Engineering, National Chiao Tung University, Hsinchu 300, Taiwan, ROC
[f] Electronics and Optoelectronics Research Laboratory, Industrial Technology Research Institute, Chutung, Hsinchu 310, Taiwan, ROC
[g] Taiwan Semiconductor Manufacturing Company, Hsinchu, Taiwan, ROC

ARTICLE INFO

Available online 17 September 2012

Keywords:
ReRAM
BON
BON:Gd
Interface type
NDR

ABSTRACT

This paper studies the effect of doping on BON-based resistive switching characteristics. Typical bipolar resistive switching behavior can be observed in Pt/BON/TiN and Pt/BON:Gd/TiN devices. The conductive path(s) of the Pt/BON/TiN is vacancy-dominated while the Pt/BON:Gd/TiN is metal-dominated. Additionally, there is an atypical bipolar resistive switching in the Gd-doping device. This atypical characteristic has not only a size effect, but also a lower operating current. The resistance transitions are due to the variation in conductance of the switching layer, which is clearly influenced by the different area size. A mechanism is proposed to explain this atypical characteristic.

© 2012 Elsevier B.V. All rights reserved.

1. Introduction

Resistive random access memory (ReRAM) has attracted considerable interest for use in the next generation of nonvolatile memory devices due to its simple structure, low operation voltage and process compatibility with the present complementary metal–oxide–semiconductor industry [1]. Many materials have been demonstrated to achieve resistive switching characteristics, such as FeO_x, Cr_2O_3, InGaZnO, and Al_2O_3 [2–8]. Two dominant resistance switching mechanisms have been proposed. One is oxygen vacancy nucleation at the metal/oxide interface [9,10]. The other mechanism is the conductive filament (CF) model, the formation/rupture of a metallic filament with a metal such as Cu or Ag acting as the mobile ions in the oxide [11]. Whether the switching mechanism is vacancy-dominated or metal-dominated, the oxygen anions and the metal atoms both play an important role in the ReRAM's switching behavior. Recently, rare earth (RE) metals, which are used broadly in the electrical and electronic industry [12,13], have been demonstrated to exhibit resistance switching phenomena [14–16]; furthermore, doping that RE metal can improve the ReRAM's characteristics [17]. Hence, in order to help clarify the influence of the metal contained in the ReRAM, this study uses the non-metal-containing BON as the base transition layer. Up to now, the application of BON in the resistive switching field has not been researched.

This work investigates resistance switching characteristics in Pt//BON/TiN and Pt//BON:Gd/TiN structures by using the temperature dependence of resistive states to observe the conductive path characteristics. The metal-doping method can provide the other resistance switching modes in the BON-based system to induce the dual switching type ReRAM. In addition, a mechanism is proposed to explain the influence on the dual switching type ReRAM.

2. Experiment

A BON thin film of 5 nm thickness was deposited on a TiN/Si substrate by reactive magnetron RF sputtering a BN target in Ar and O_2 ambient at room temperature. The RF sputtering power, time and pressure of the sputter system were set to 80 W, 800 s, and 1066 Pa. Next, the Pt top electrode (TE) was deposited and patterned by the liftoff process. In addition, the fabrication of the Pt/BON:Gd (10%)/TiN structure was similar to the Pt/BON/TiN structure, which was formed by co-sputtering the BON and Gd targets with the same deposition conditions as that for the Pt/BON/TiN structure. Fourier transform infrared spectrometry (FTIR) transmission spectra were used to observe the composition of BON and BON:Gd films by Bruker VERTEX 70v Fourier Transform Infrared Spectroscopy. The standard sample was a Pt/BON/TiN (PBT) structure, whereas the control sample used as reference was the Pt/BON:Gd/TiN (PBGT) structure, and

* Corresponding author at: Department of Physics, National Sun Yat-Sen University, Kaohsiung, 804, Taiwan, ROC. Tel.: +886 3 5726100; fax: +886 3 5722715.
E-mail address: tcchang@mail.phys.nsysu.edu.tw (H.-C. Tseng).

0040-6090/$ – see front matter © 2012 Elsevier B.V. All rights reserved.
http://dx.doi.org/10.1016/j.tsf.2012.09.031

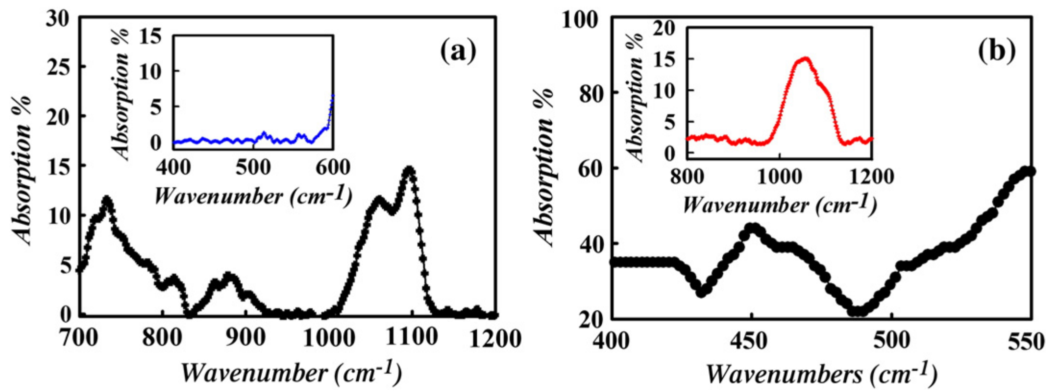

Fig. 1. Fourier transform infrared spectrometry (FTIR) transmission spectra of (a) BON film in M-IR region, and (b) BON:Gd film in far-IR region. Insets of (a) and (b) show BON film in Far-IR region and BON:Gd film in M-IR region.

will be referred to as PBT and PBGT samples hereafter. Additionally, both the PBT and PBGT samples needed to be activated by electroforming with a positive bias treatment about 5 V. All electrical characteristics were measured over an 8 μm × 8 μm to 2 μm × 2 μm cell size with an Agilent B1500 semiconductor parameter analyzer. During these measurements, bias was applied to the TiN bottom electrode (BE) while the Pt top electrode (TE) was ground.

3. Results and discussion

Many studies have indicated that the ReRAM characteristic is due to the redox process by cation or anion migration, which is strongly related to oxygen or metal ions. In order to clarify the influence between oxygen and metal ions for ReRAM switching behaviors, this study uses the BON thin film with and without Gd doping as the insulator. Fig. 1 shows the FTIR transmission spectra analysis which can be examined for the composition of the PBT and PBGT device transition layers. Fig. 1(a) shows that the bonds around 792 and 1064 and 1083 (cm^{-1}), respectively, are due to the H-BN, the C-BN and the B-O-B stretching vibration for the PBT device [18,19]. The inset of Fig. 1(a) shows that there are no chemical bond signals around the Far-IR spectrum region. Furthermore, Fig. 1(b) shows that the bonds around 440 and 542 (cm^{-1}) represent the Gd–O vibration of cubic Gd_2O_3 for the PBGT device [20]. The inset of Fig. 1(b) also shows the C-BN and B-O-B bonds for the PBGT device.

Fig. 2(a) shows the typical bipolar switching behavior for the PBT and PBGT devices under identical operation conditions. The transitions between low resistance state (LRS) and high resistance state (HRS) are observed for 100 cycles by using dc voltage sweeping mode, as shown in insets (i) and (ii) of Fig. 2(a). Both PBT and PBGT devices require activation by the electroforming process. The resistance can be switched to HRS by applying negative bias of about −2 V. In a subsequent sweep, the RS can be switched again to LRS by applying a predetermined positive bias of about 2 V with a 10 mA current compliance (I_{com}). The temperature dependence of the LRS for the PBT and PBGT devices is shown in Fig. 2(b), which indicates that the LRS of the PBT device decreases as ambient temperature increases, as is typical of semiconductor behavior properties [14]. This implies that the CF is dominated by vacancies. In contrast, the LRS for the PBGT device increases as ambient temperature rises, which indicates a typical metallic behavior [14]. These results support that doping BON with Gd can transform the CF from vacancy-dominated to metallic-Gd dominant.

Recent studies have indicated that the bipolar resistance switching is related to the redox reaction near the anode–electrode/oxide interface, which can be also defined as the switching layer (SL) [14,21,22]. Fig. 3(a) and (b) shows the size effect of the PBT and PBGT devices, respectively. The CF cannot connect the top electrode (TE) and the bottom electrode (BE) undergoing the reset process. Hence, the leakage can be proportional to the device area. In contrast, there are no obvious trends when comparing leakage and area during the set process because the TE and BE have been connected by the CF. No matter whether the CF is vacancy-dominated or metallic-Gd dominant, the size effect of the off-current is due to the SL area size; moreover, the set process is a local behavior causing there to be no clear area dependence for the on-current.

According to the PBGT device results found in Fig. 2(b), using the multilevel measurement for LRS re-confirms the metallic-Gd dominant CF. Fig. 4(a) shows that applying different I_{com} during the set process, such as 1 mA, 5 mA, 10 mA, and 15 mA, induces the multi-on states. Accordingly, inset of Fig. 4(a) shows that the temperature dependence of the multi-on state increases as ambient temperature rises. Because the CF's diameter or conductance is proportional to the I_{com} [23], a higher I_{com} accompanies higher conductance for the CF [24]. In addition, Fig. 4(b) shows that the PBGT device has an

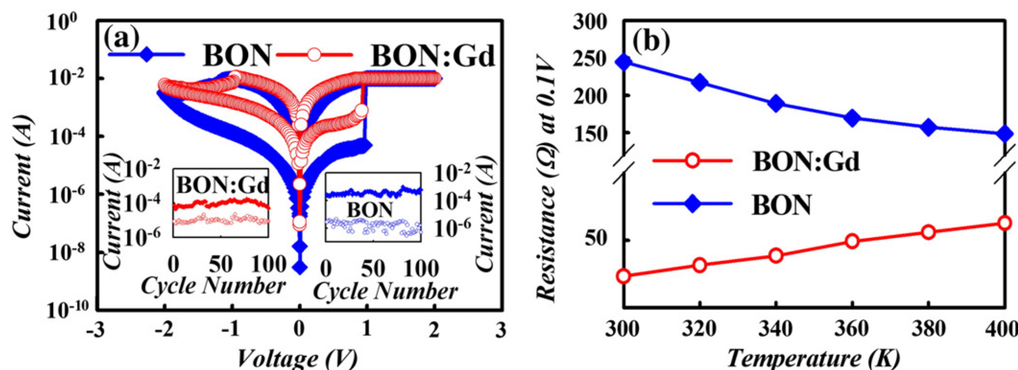

Fig. 2. (a) Typical bipolar resistive switching I–V curves for the BON and BON:Gd devices. (b) Temperature dependence of resistance in LRS for the BON and BON:Gd devices, with a 0.1 V reading voltage.

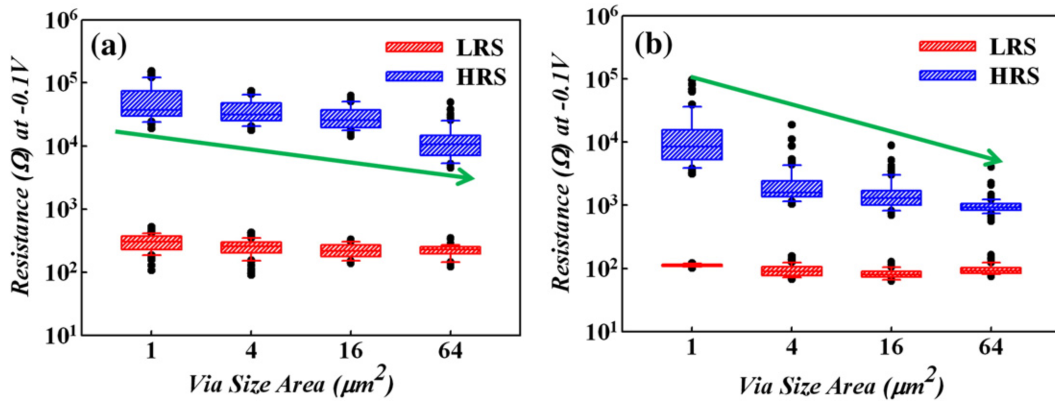

Fig. 3. Size effect of LRS/HRS for (a) Pt/BON/TiN device and (b) Pt/BON:Gd/TiN device.

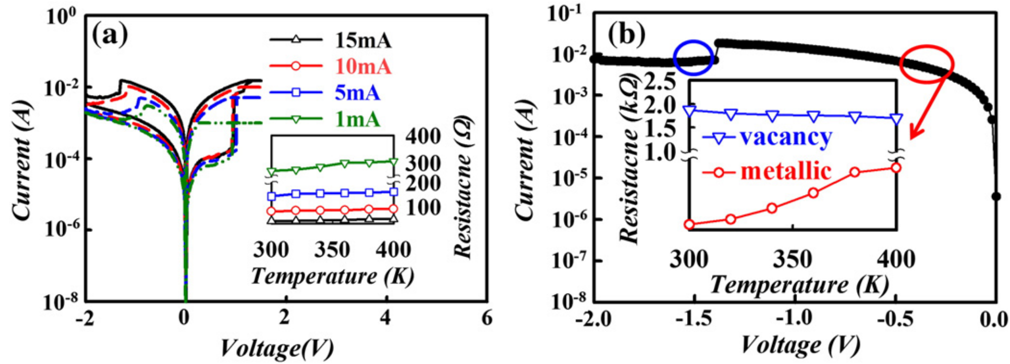

Fig. 4. (a) Typical bipolar resistive switching I–V curves for BON:Gd devices with different current compliance, and (b) reset process for the BON:Gd device. Inset of (a) shows the temperature dependence of the multi-LRS, and inset of (b) shows the temperature dependence of the LRS and middle-LRS.

unusual trend when comparing the reset-voltage region of the PBT and PBGT devices. As a higher I_{com} is applied, there is a sudden obvious transformation from LRS to middle-LRS. The different temperature dependencies of the LRS and the middle-LRS are also shown in the inset of Fig. 4(b). Comparing the on- and off-current values reveals that the leakages for the PBGT device are higher than the PBT device due to the doping metal effect. Undergoing the reset process, the applied-voltage prefers to act on the metallic-type CF. After the sudden transformation, the conductance of the metallic CF becomes low enough to cause the applied-voltage to act on the vacancy-type CF instead. Regardless of whether the CF is vacancy-dominated or metallic-Gd dominated, the resistance transition can be defined as a filament type resistive switching behavior.

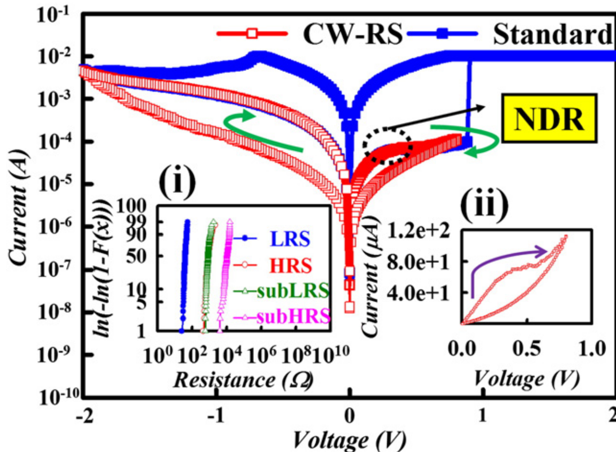

Fig. 5. Untypical bipolar resistive switching I–V curves (CW-RS) for the BON:Gd device. The inset (i) shows the on/off ratio for standard-RS and CW-RS, and (ii) shows the ND-HRS.

However, compared with other ReRAM characteristics [25,26], a particular behavior for the PBGT device during resistance switching exhibits a negative differential resistance (NDR) at the HRS while applying positive bias as shown in the inset (ii) of Fig. 5. This phenomenon is similar to the standard reset process of the bipolar switching cycles. In order to examine whether the NDR at HRS (NDR_{HRS}) possesses a memory window, the sweeping voltage is applied from 0 V → +0.8 V →−2 V → 0 V. There is a clockwise (CW) parasitic switching, and the sub-LRS/sub-HRS switching (sub-LRS is equal to standard-HRS) is below HRS of the standard ReRAM, as shown in Fig. 5. In addition, the sub-LRS/sub-HRS ratio is sufficient to be distinguished during 100 dc bias switching cycles, as shown in the inset (i) of Fig. 5. These results also show that this CW resistance switching (CW-RS) mode not only reduces operation voltages such as V_{set} and V_{reset}, but also improves the operating current. The CW-RS mode, therefore, has potential applications in low power portable electronic products.

Confirmation of the path characteristics can be achieved by using the temperature dependence of the resistance state for sub-LRS and sub-HRS. Fig. 6(a) shows that both the sub-LRS and sub-HRS decrease when the ambient temperature increases, which indicates that the CW-RS is typically semiconductor-like. Hence, the switching behaviors are related to the conductance variation of SL. As the state has not switched to LRS yet during the set process, the electric field still slightly drives the mobile oxygen anions. This effect prefers to occur near the SL/metallic-type CF region due to the high conductance of metallic CF. This phenomenon causes few oxygen anions to drift to the SL region; moreover, the oxygen anions may accumulate and recombine with the oxygen vacancies forming a more insulated SL [27]. Subsequently, the SL conductance can become lower, causing

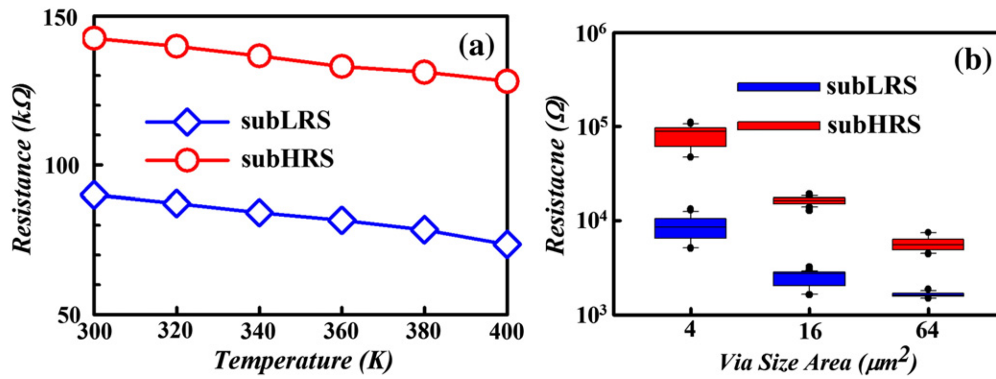

Fig. 6. (a) Temperature dependence for sub-LRS and sub-HRS, and (b) size effect for sub-LRS and sub-HRS.

the leakage current decrease which typifies NDR_{HRS} behavior. Therefore, the SL oxidation effect should be related to the area size, as shown in Fig. 6(b). The current transformation of the CW-RS mode is attributed to the conductance variation for SL under the small electric field, so there is indeed a size effect for sub-LRS and sub-HRS. The CW-RS mode can then be defined as interface type resistive switching behavior [28–30].

The results of current fitting indicate that the sub-LRS and sub-HRS for the CW-RS obey the Schottky conduction mechanism, as shown in Fig. 7(b) and (c). Gibb's free energy change accompanying the solution of the oxygen in the Gd and Ti has been studied, which indicates that the oxygen affinity of Gd is higher than Ti [31]. Since the TiN is regarded as the buffer layer blocking and attracting the oxygen ions, the mobile oxygen ions can accumulate among the SL region of TiN/bulk (residual filament) which has undergone the positive bias treatment and the filament-type RS has not been triggered yet. Then, the accumulated oxygen ions can oxidize the Gd and form a temporary barrier oxide due to the higher Gibb's free energy of Gd. Accordingly, the transition current become lower. Moreover, if there is no Schottky barrier formation, the soft break down voltage (set process of filament type ReRAM) should be located at Vset′. However, Gd attracting the oxygen ion induces the barrier formation, causing a shift of the set voltage (Vset). Therefore, the sweeping condition treated within the Vset of filament type ReRAM induces a reset behavior for the CW-RS. In a subsequent sweep, the reverse polarity bias can drive the oxygen ions back to the residue filament region due to the temporary barrier annihilation. Owing to the formation and deformation of the Schottky barrier, the CW-RS behavior can be achieved.

4. Conclusion

In conclusion, an investigation of the effect of a BON insulator layer with and without doped metal indicates that vacancy-type CF always exists in the Pt/BON/TiN and Pt/BON:Gd/TiN devices, with the metallic-type CF only appearing in the metal-doped device. Furthermore, the metal-doping device induces a dual-switching type device causing there to two trends in resistance switching, namely filament-type and interface-type. The formation and deformation of the Schottky barrier, result in the interfacial-type ReRAM. The interfacial-type ReRAM not only has lower switching voltages such as V_{set} and V_{reset}, but also reduces the operating leakage, which improves the ReRAM's power consumption. Finally, if the size area can be scaled down sufficiently, operating current can be further reduced without an increase in switching voltages.

Acknowledgment

This work was performed at the National Science Council Core Facilities Laboratory for Nano-Science and Nano-Technology in Kaohsiung-

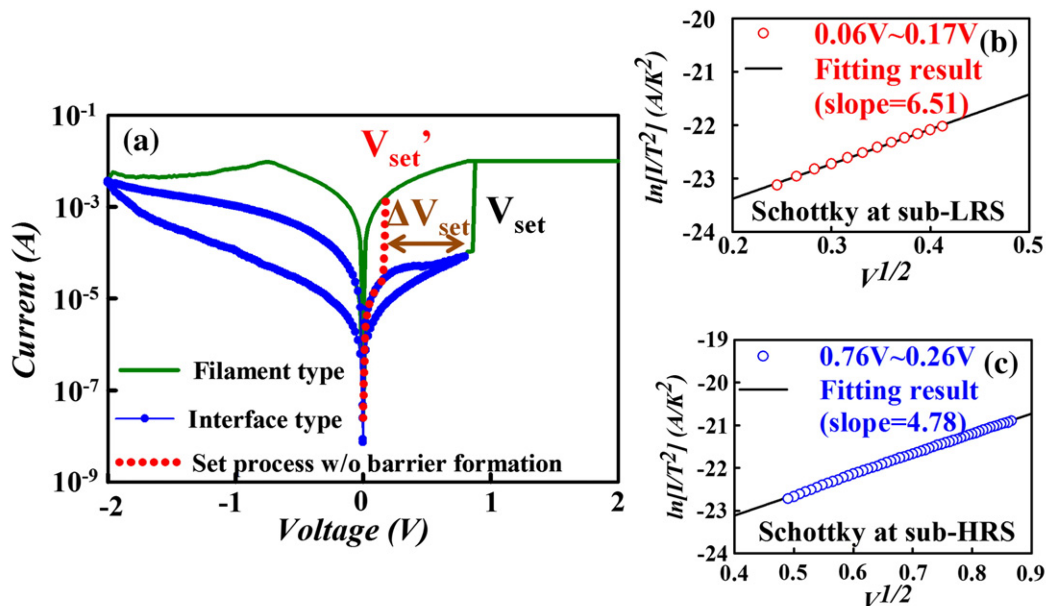

Fig. 7. (a) Set voltage shift for BON:Gd devices. Current fitting results of Schottky conduction mechanism for (b) sub-LRS and (c) sub-HRS.

Pingtung area and was supported by the National Science Council of the Republic of China under Contract Nos. NSC-100-2120-M-110-003.

References

[1] K. Szot, W. Speier, G. Bihlmayer, R. Waser, Nat. Mater. 5 (4) (2006) 312.
[2] L.W. Feng, C.Y. Chang, Y.F. Chang, W.R. Chen, S.Y. Wang, P.W. Chiang, T.C. Chang, Appl. Phys. Lett. 96 (2010) 052111.
[3] L.W. Feng, C.Y. Chang, Y.F. Chang, T.C. Chang, S.Y. Wang, S.C. Chen, C.C. Lin, S.C. Chen, P.W. Chiang, Appl. Phys. Lett. 96 (2010) 222108.
[4] L.W. Feng, Y.F. Chang, C.Y. Chang, T.C. Chang, S.Y. Wang, P.W. Chiang, C.C. Lin, S.C. Chen, S.C. Chen, Thin Solid Films 519 (2010) 1536.
[5] S.C. Chen, T.C. Chang, S.Y. Chen, H.W. Li, Y.T. Tsai, S.M. Sze, F.S. Yeh (Huang), Y.H. Tai, Electrochem. Solid-State Lett. 14 (2) (2011) H103.
[6] M.C. Chen, T.C. Chang, C.T. Tsai, S.Y. Huang, S.C. Chen, C.W. Hu, S.M. Sze, M.J. Tsai, Appl. Phys. Lett. 96 (2010) 262110.
[7] M.C. Chen, T.C. Chang, S.Y. Huang, S.C. Chen, C.W. Hu, C.T. Tsai, S.M. Sze, Electrochem. Solid-State Lett. 13 (6) (2010) H191.
[8] Y.T. Tsai, T.C. Chang, C.C. Lin, S.C. Chen, C.W. Chen, S.M. Sze, F.S. Yeh (Hung), T.Y. Tseng, Electrochem. Solid-State Lett. 14 (3) (2011) H135.
[9] J.J. Yang, F. Miao, M.D. Pickett, D.A.A. Ohlberg, D.R. Stewart, C.N. Lau, R.S. Williams, Nanotechnology 20 (2009) 215201.
[10] C. Yoshida, K. Kinoshita, T. Yamasaki, Y. Sugiyama, Appl. Phys. Lett. 93 (2008) 042106.
[11] C. Schindler, G. Staikov, R. Waser, Appl. Phys. Lett. 94 (2009) 072109.
[12] A. Fissel, M. Czernohorsky, H.J. Osten, Superlattices Microstruct. 40 (2006) 551.
[13] L. Marsella, V. Fiorentini, Phys. Rev. B 69 (2004) 172103.
[14] H.C. Tseng, T.C. Chang, J.J. Huang, P.C. Yang, Y.T. Chen, F.Y. Jian, S.M. Sze, M.J. Tsai, Appl. Phys. Lett. 99 (2011) 132104.
[15] K.C. Liu, W.H. Tzeng, K.M. Chang, Y.C. Chan, C.C. Kuo, C.W. Cheng, Microelectron. Reliab. 50 (2010) 670.
[16] S.Y. Huang, T.C. Chang, M.C. Chen, S.C. Chen, H.P. Lo, H.C. Huang, D.S. Gan, S.M. Sze, M.J. Tsai, Solid-State Electron. 63 (2011) 189.
[17] H. Zhang, L. Liu, B. Gao, Y. Qiu, X. Liu, J. Lu, R. Han, J. Kang, B. Yu, Appl. Phys. Lett. 98 (2010) 042105.
[18] J. Ye, S. Ulrich, C. Ziebert, M. Stüber, Thin Solid Films 517 (2008) 1151.
[19] Q. Yang, J. Shab, L. Wanga, Y. Zoua, J. Niua, C. Cuia, D. Yang, Physica E 27 (2005) 319.
[20] H. Guo, N. Dong, M. Yin, W. Zhang, L. Lou, S. Xia, J. Phys. Chem. B 108 (50) (2004) 19205.
[21] Y.E. Syu, T.C. Chang, C.T. Tsai, G.W. Chang, T.M. Tsai, K.C. Chang, Y.H. Tai, M.J. Tsai, S.M. Sze, Electrochem. Solid-State Lett. 14 (10) (2011) H419.
[22] Y.E. Syu, T.C. Chang, T.M. Tsai, Y.C. Hung, K.C. Chang, M.J. Tsai, M.J. Kao, S.M. Sze, IEEE Electron Device Lett. 32 (4) (2011) 545.
[23] K.M. Kim, C.S. Hwang, Appl. Phys. Lett. 94 (2009) 122109.
[24] Y.F. Chang, T.C. Chang, C.Y. Chang, J. Appl. Phys. 110 (2011) 053703.
[25] P.C. Yang, T.C. Chang, S.C. Chen, Y.S. Lin, H.C. Huang, D.S. Gan, Electrochem. Solid-State Lett. 14 (2) (2011) H93.
[26] S.C. Chen, T.C. Chang, S.Y. Chen, C.W. Chen, S.C. Chen, S.M. Sze, M.J. Tsai, M.J. Kao, F.S.Y. Huang, Solid-State Electron. 62 (2011) 40.
[27] Y.T. Tsai, T.C. Chang, W.L. Huang, C.W. Huang, Y.E. Syu, S.C. Chen, S.M. Sze, M.J. Tsai, T.Y. Tseng, Appl. Phys. Lett. 99 (2011) 092106.
[28] R. Muenstermann, T. Menke, R. Dittmann, R. Waser, Adv. Mater. 22 (2010) 4819.
[29] K.P. Biju, X. Liu, S. Kim, S. Jung, J. Park, H. Hwang, Phys. Status of Solidi RRL 5 (3) (2011) 89.
[30] F. Miao, J.J. Yang, J. Borghetti, G. Medeiros-Ribeiro, R.S. Williams, Nanotechnology 22 (2011) 254007.
[31] T.H. Okabe, K. Hirota, E. Kasai, F. Saito, T. Waseda, K.T. Jacob, J. Alloys Compd. 279 (1998) 184.